**Earth Surface Processes and Landforms**
*Earth Surf. Process. Landforms* (in press)
Published online in Wiley InterScience (www.interscience.wiley.com). **DOI:** 10.1002/esp.1246

# Spatial structures of stream and hillslope drainage networks following gully erosion after wildfire

John A. Moody[1]* and David A. Kinner[2]
[1] *US Geological Survey, 3215 Marine Street, Suite E-127, Boulder, CO 80303, USA*
[2] *US Geological Survey, PO Box 25046, Mail Stop 966, Denver, CO 80225, USA*

**Correspondence to:*
*J. A. Moody, US Geological Survey, 3215 Marine Street, Suite E-127, Boulder, CO 80303, USA.*
*E-mail: jamoody@usgs.gov*

Received 13 July 2004;
Revised 23 February 2005;
Accepted 4 April 2005

## Abstract

**The drainage networks of catchment areas burned by wildfire were analysed at several scales. The smallest scale (1–1000 $m^2$) representative of hillslopes, and the small scale (1000 $m^2$ to 1 $km^2$), representative of small catchments, were characterized by the analysis of field measurements. The large scale (1–1000 $km^2$), representative of perennial stream networks, was derived from a 30-m digital elevation model and analysed by computer analysis.**

**Scaling laws used to describe large-scale drainage networks could be extrapolated to the small scale but could not describe the smallest scale of drainage structures observed in the hillslope region. The hillslope drainage network appears to have a second-order effect that reduces the number of order 1 and order 2 streams predicted by the large-scale channel structure. This network comprises two spatial patterns of rills with width-to-depth ratios typically less than 10. One pattern is parallel rills draining nearly planar hillslope surfaces, and the other pattern is three to six converging rills draining the critical source area uphill from an order 1 channel head. The magnitude of this critical area depends on infiltration, hillslope roughness and critical shear stress for erosion of sediment, all of which can be substantially altered by wildfire. Order 1 and 2 streams were found to constitute the interface region, which is altered by a disturbance, like wildfire, from subtle unchannelized drainages in unburned catchments to incised drainages. These drainages are characterized by gullies also with width-to-depth ratios typically less than 10 in burned catchments. The regions (hillslope, interface and channel) had different drainage network structures to collect and transfer water and sediment.** 

**Keywords: channels; drainage networks; gully; hillslopes; wildfire; scaling; stream networks**

## Introduction

Wildfires are landscape-scale disturbances that change the hydrologic and erosional response of catchment areas. When significant rainfall follows a wildfire, the subsequent runoff and erosion can expand the existing pre-fire channel network (Moody and Martin, 2001a). With an increase in wildfire throughout the wildland–urban interface in the western United States and elsewhere, a need exists to model the drainage networks of burned catchments in order to predict floods. Only after the unsteady flood flow problem is modelled correctly in burned catchments, can the associated spectrum of sediment erosion, transport and deposition processes (which includes debris flows) be modelled.

One fundamental question related to post-fire erosion is how the new drainage networks are similar to or different from the pre-fire channel network. If the new drainage network follows previously defined but subtle drainages (i.e. unchannelized drainages without definite banks), then it is possible that the larger channel structure is preserved. However, it also is possible that the new drainage network may have a different structure, particularly in the area linking hillslope and channel regions. This area where subtle drainages connect the hillslope region (planar or convex surfaces) with the channel region (drainages with definite banks) will be referred to in this paper as the interface region, which is essentially the same as the zone of transition described by Montgomery and Dietrich (1994).

Modelling runoff from burned catchments is problematic because (1) it is difficult to predict the drainage structure of the newly eroded terrain, (2) existing runoff prediction models have not been designed for unsteady flow typical of

burned catchments, and (3) existing empirical techniques for predicting runoff in ungauged, unburned catchments (Interagency Advisory Committee on Water Data, 1981; Jennings *et al*., 1994; Vail, 2000) have not been verified for burned mountainous catchments. One way to simplify modelling of runoff from burned catchments areas is to apply both similarities in topography and scaling properties. Scale refers to a characteristic time or length (Blosch, 1999) that controls a physical process while scaling laws establish the relations between two variables under a change in scale (Dodds and Rothman, 2000) and are typically power laws in form (for example Hack's law; Hack, 1957; Dodds and Rothman, 2000). Geometric or self-similarity implies that the structure of the process or the river basin is the same regardless of scale (Mandelbrot, 1967, Peckham, 1995a). An excellent example of a landscape-scale similarity relation that has been applied to simplify the modelling process is the physically based hydrologic model TOPMODEL (Beven and Kirkby, 1979). In the model, areas with a common value of the topographic parameter $\ln(a/S)$ (drainage area per contour width, $a$ (m), per local slope, $S$) perform the same in model calculations. This approach reduces the computational requirements of the model and takes advantage of the replication of topographic structures throughout a landscape.

Descriptions of the spatial structure of channel networks have been limited to one- and quasi-two-dimensional variables. Horton (1945) initially developed one-dimensional *laws of drainage composition* in the form of ratios of stream variables (stream number or bifurcation ratio, stream lengths and stream slopes), which are empirical descriptors of the change in drainage structure with scale along one dimension, which follows a stream channel. Rodriguez-Iturbe and Rinaldo (1997) later expanded Horton's empirical work and investigated optimal channel networks determined by the physical principle of minimum energy expenditure (Leopold and Langbein, 1962; Howard, 1990) but still followed a stream channel limiting the study to one dimension. Shreve (1966, 1969) proposed that the evolution of channel networks in a particular lithology or similar geological terrain is a random process and as a consequence would have a theoretical bifurcation ratio of 4·0. Despite the apparent utility of Horton ratios, their ability to differentiate stream networks has been debated (Kirchner, 1993; Troutman and Karlinger, 1994). These one-dimensional descriptors of channel networks have been augmented by Moody and Troutman (2002) who studied the two-dimensional characteristics (width and depth) of a channel but still as a function of distance along the stream channel (one dimension). However, Tokunaga (1978) and later Peckham (1995b) suggested a variable $T_{\omega,k}$, to describe the topological spatial structure of channel networks. The value of $T_{\omega,k}$ is equal to the average number of side tributaries of order $k$ entering a stream of order $\omega$ and does not include the streams of order $k$ that form a stream of order $k+1$. These variables form a square, lower triangular matrix (referred to in this paper as the Tokunaga matrix), and this Tokunaga matrix describes the total branching (quasi-two-dimensional) structure of the entire channel network.

The structure of hillslope drainage networks differs from the structure of channel networks. Hillslopes are not scale-invariant as has been shown for channel networks (Rodriguez-Iturbe and Rinaldo, 1997), but appear to have at least three fundamental scales. One is the length scale identified by Horton (1945) as the 'critical distance' for the initiation of erosion, a second is the roughness scale identified by Andrle and Abrahams (1989), and a third scale is the critical area (within the interface region) necessary for the development of channels. Theoretical hillslopes were explicitly defined by Sun *et al*. (1994) as those surfaces with constant inclination and a threshold criterion that the area is less than the critical area for channel initiation per unit rainfall intensity (Montgomery and Dietrich, 1994). Tucker and Bras (1998) expanded this simple criterion by investigating several different hillslope (or channel) threshold criteria.

Our purpose is to examine similarities in channel networks with an eye toward simplifying process models, and to determine the spatial structure of the drainage networks within the hillslope, interface and channel regions in a catchment following gully erosion after wildfire. We rely on both field studies and computer analysis to: (1) examine the drainage structures of the post-fire hillslope, interface, and channel regions; (2) compare them to the structure of the networks in unburned catchments derived from computer analysis of large-scale (1–1000 $km^2$) digital elevation models; (3) explore how the channel network interfaces with the hillslope network; and (4) determine if either the spatial structure or channel thresholds have changed as a consequence of the wildfire disturbance.

## Background

The 1996 Buffalo Creek Fire burned approximately 50 $km^2$ of two adjacent mountainous catchment areas (Buffalo Creek and Spring Creek) southwest of Denver, Colorado. A larger proportion of the Spring Creek catchment burned (79 per cent or 21·2 $km^2$) compared with the Buffalo Creek catchment (21 per cent, 25·7 $km^2$). These catchments are underlain by the Pikes Peak granite batholith (Figure 1) and soils are classified as Typic Ustorthents on south-facing hillslopes and as Typic Cryorthents on north-facing hillslopes (Blair, 1976; Moore, 1992; Welter, 1995). Depths to

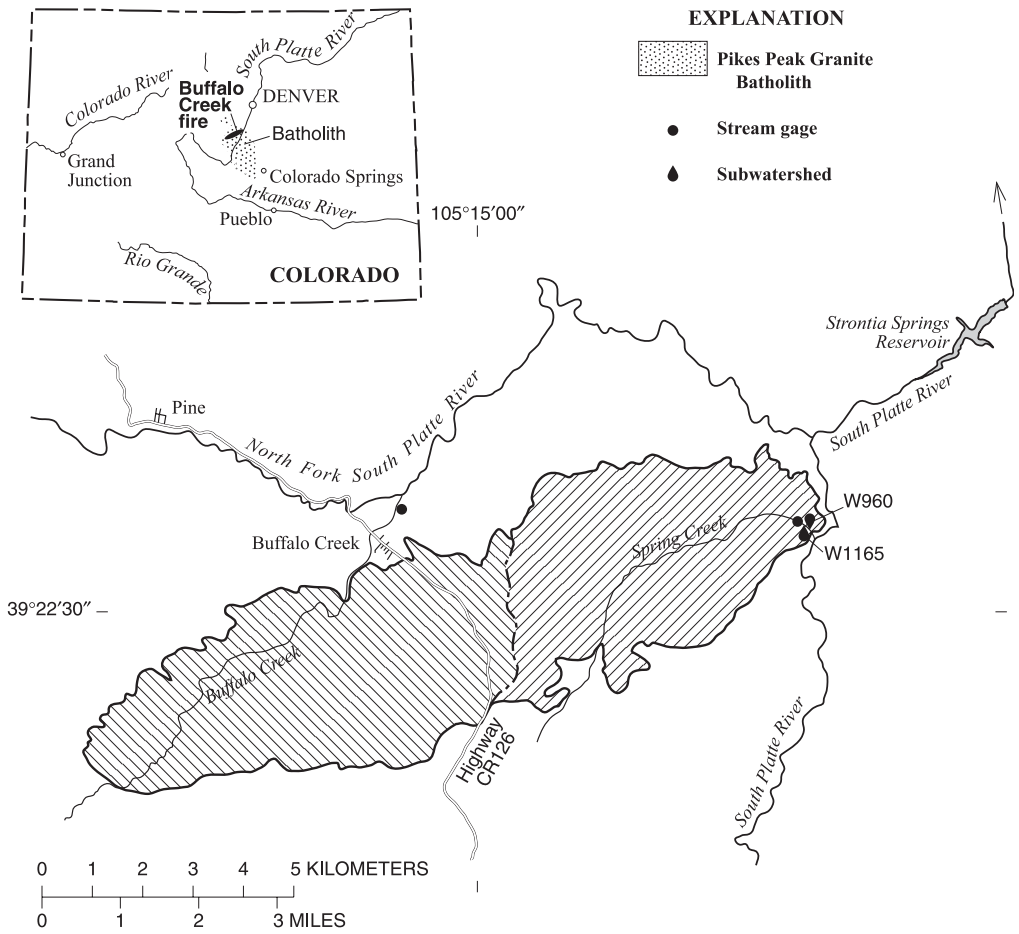


**Figure 1.** Location of the two subcatchments (W960 and W1165) in the Spring Creek catchment burned by the 1996 Buffalo Creek Fire (shown by cross-hatching) within the Pikes Peak granite batholith.

bedrock are quite variable, and the soil profile in the regolith includes emerging corestone and thick layers of decomposed granite called grüs.

Two short-duration, high-intensity rainstorms after the wildfire created runoff that altered the topography of the hillslope, interface and channel regions. Both storms (12 July 1996 and 31 August 1997) lasted about one hour and had a maximum rainfall intensity of about 90 mm $h^{-1}$ (Moody and Martin, 2001a). The runoff removed most of the ash from the hillslopes, rilled the hillslope surfaces, channelized subtle drainages constituting the interface region, which led to a headward extension of the channel network into previously uneroded terrain, and deposited sediment in channels. Two subcatchments, referred to as W960 and W1165 (the number equals the distance from the mouth of Spring Creek), were investigated to determine the amount of erosion (Moody and Martin, 2001b) and the drainage network structure in the newly eroded terrain (Figure 2). Subcatchment W960 (7·01 ha) is a south-facing catchment with an estimated hillslope length (1/(2 × drainage density); Horton, 1945) of 24 m and W1165 (3·71 ha) is a north-facing catchment with hillslope length of 10 m.

## Methods

Topologic variables were measured at both the large scale (1–1000 $km^2$) from a 30-m digital elevation model (DEM) and at smaller scale (1–1000 $m^2$) in the field. Hydraulic and dynamic variables were only measured in the field at the smaller scales.

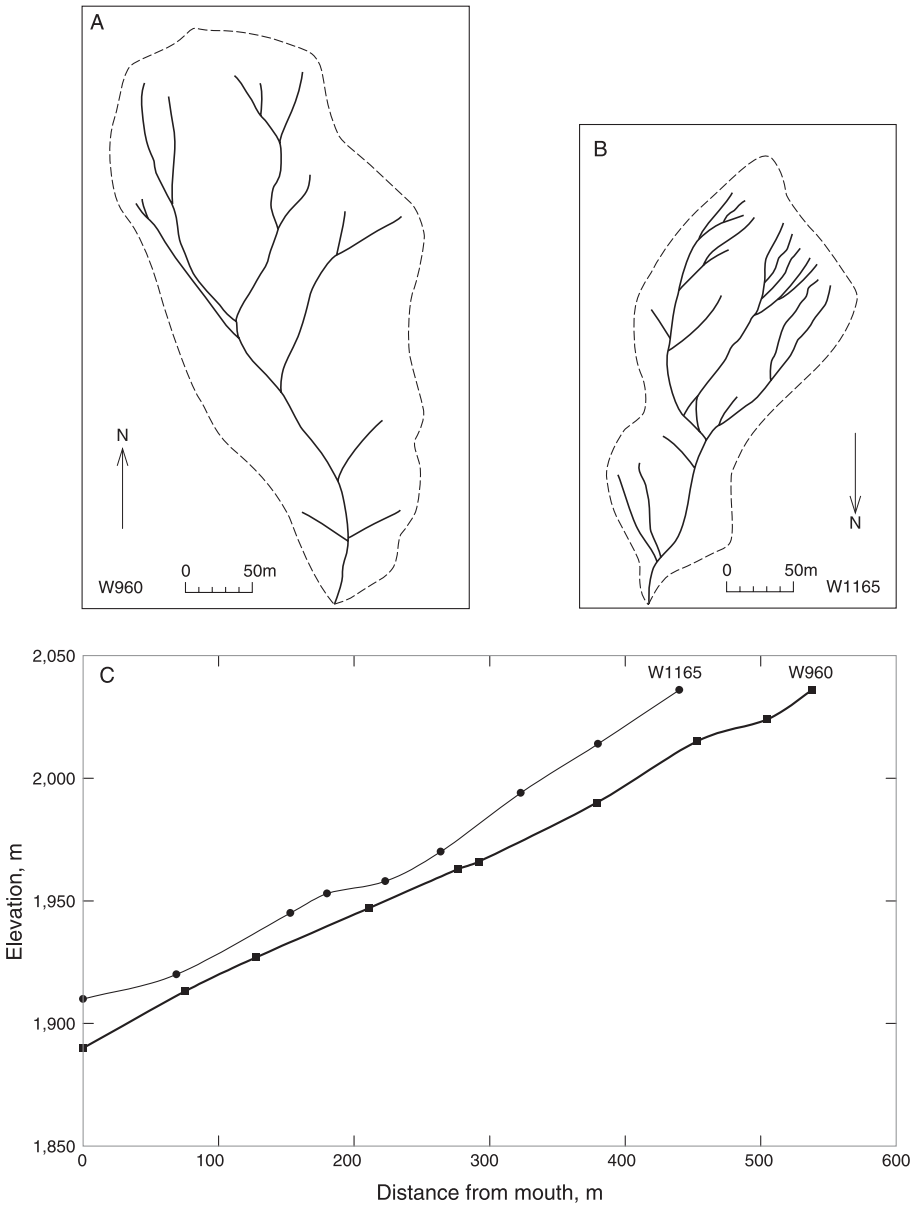


**Figure 2.** (A) Drainage network for subcatchment W960. (B) Drainage network for subcatchment W1165. (C) Longitudinal profiles following the longest stream path in catchments W960 and W1165.

## Drainage network calculations

The one-dimensional Horton ratios were computed for three different scales (subcatchment, Spring Creek and Pikes Peak granite batholith; Figure 3). The Horton ratio, $R_X$, for a stream variable, $X$, has the general form for streams of orders $\omega$ and $k$:

$$R_X^{|\omega-k|} = \frac{X_\omega}{X_k} \tag{1}$$

where for the bifurcation ratio, $R_B$, $X_\omega$ decreases with increase in $\omega$ and for the other ratios ($R_A$, drainage area; $R_L$, stream length; $R_w$, stream width) $X_\omega$ increases with increase in $\omega$ (Peckham and Gupta, 1999). In the Horton–Strahler

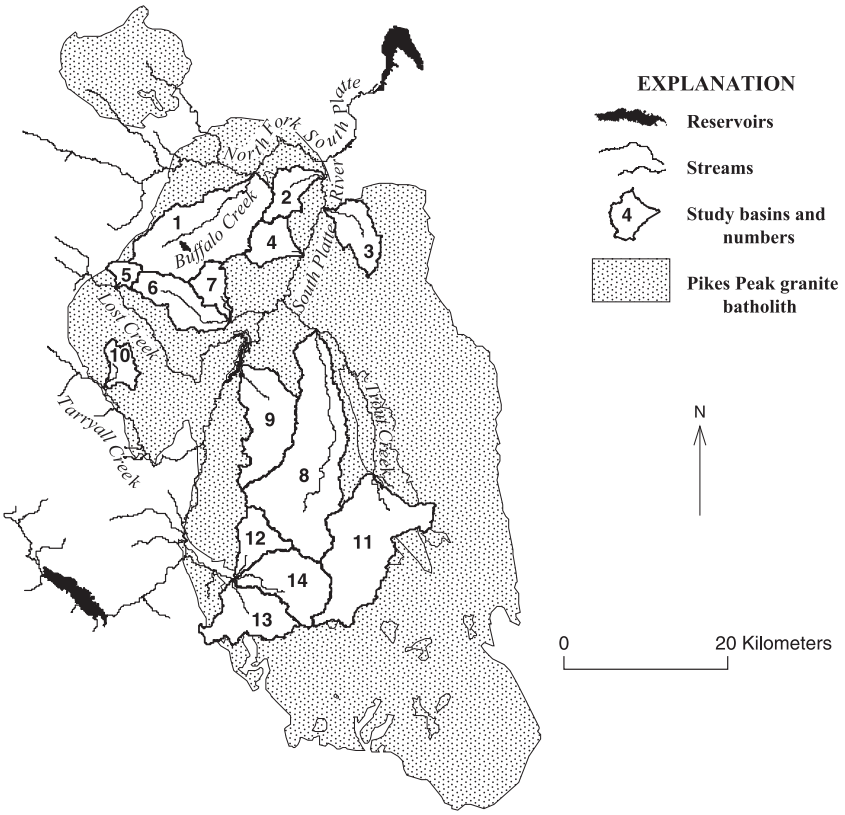


**Figure 3.** Location of the 14 order 6 catchments within the boundaries of the Pikes Peak granite batholith.

stream order system (Strahler, 1957; Peckham and Gupta, 1999), channels with no upstream tributaries are considered order 1 streams and if two streams of order $\omega$ join, they form a stream of order $\omega + 1$ (if a stream of a given order joins a higher order stream, then the stream order does not change). The average Horton ratio can be more easily calculated by making the mathematical substitution (Knighton, 1998)

$$R_X = \frac{c}{|c|} e^{|c|} \tag{2}$$

which yields an estimate of $R_X$ from the regression slope $c$ for a log-linear plot of the stream variable $X$ versus stream order $\omega$. An additional advantage of this substitution is that a positive slope $c$ indicates a proportional relation between $X$ and $\omega$ and a negative slope indicates an inverse relation (Table I). The fractal dimension was computed as the ratio of $R_B/R_L$. Horton ratios tend to increase with the scale of a catchment, approaching an asymptotic value in larger catchment areas (Peckham, 1995a). Thus, ratios computed for catchments with only a few stream orders may be less than the asymptotic value.

To compare the structure of larger catchments with the structure of the small subcatchments, we investigated the self-similarity of the drainage networks using the Tokunaga matrix. Peckham (1995b) has suggested that one measure of self-similarity in a channel network is that the elements along diagonals in the Tokunaga matrix are identical, $T_{\omega,\omega-k} = T_k$. For example if $T_{2,1} \sim T_{3,2} \sim T_{4,3}$ are identical, or nearly so, they can be replaced by a single value, $T_1$. Similarity implies that the drainage network repeats its structure at many scales, and the stream numbers can then be calculated from the following recursive relation (Peckham, 1995a)

$$N_\omega = 2N_{\omega+1} + \sum_{k=1}^{\Omega-\omega} T_k N_{\omega+k} \tag{3}$$

where $N_\Omega$ is the highest order stream and is equal to 1.

**Table I.** Average Horton ratios for three different spatial scales

| Variable | Symbol | Pikes Peak granite batholith | Spring Creek | W960 | W1165 |
|---|---|---|---|---|---|
| Topologic variables | | | | | |
| Bifurcation | $R_B$ | −4·3 | −3·7 | −3·6 | −2·6 |
| Drainage area | $R_A$ | 4·8 | 4·0 | 5·9 | 3·8 |
| Length | $R_L$ | 2.3 | 1·9 | 2·5 | 1·6 |
| Slope | $R_S$ | −1·4 | −1·3 | −1·4 | −1·2 |
| Fractal dimension | $D$ | 1·9 | 1·9 | 1·4 | 1·6 |
| Hydraulic variables | | | | | |
| Width | $R_{wT}$ | na | na | 2·3 | 1·9 |
| Depth | $R_h$ | na | na | 2·1 | 1·4 |
| Cross-sectional area | $R_a$ | na | na | 5·0 | 2·7 |
| Bed roughness | $R_{z0}$ | na | na | −1·1 | −1·0 |
| Width-to-depth ratio | $R_{w/h}$ | na | na | −1·2 | 1·4 |
| Dynamic variable | | | | | |
| Catchment Froude number | $R_F$ | na | na | 1·0 | 1·0 |

na, Not available; negative sign indicates variable decrease as stream order increases

## Large-scale measurements

Large-scale topologic analysis of stream networks was completed using a single composite 30-m DEM (hereafter, composite DEM) with a grid cell resolution of 900 $m^2$. The composite DEM comprised 36, 7·5-minute quadrangles joined together by using the program RiverTools (Peckham, 1998; Rivix LLC, 2001). This composite DEM encompassed the topography of much of the Pikes Peak granite batholith, which was determined from the digital geological map of Green (1992) projected to match the projection of the composite DEM (UTM, zone 13, datum = NAD27). Because of the difference in initial projection and the large-scale nature of the geological map (1:500 000), the boundaries of the batholith shown in Figure 3 are approximate in nature. We used the D-8 flow direction algorithm (O'Callahan and Mark, 1984) and iterative linking flat resolution (Jenson and Domingue, 1988) in order to determine flow directions on the DEM. Streams were differentiated from surrounding hillslopes by using a critical area of 0·01 $km^2$ (1 ha) and the structure of the drainage network was analysed using RiverTools. The selected critical area is consistent with the long-term average area for unburned catchments shown by Montgomery and Dietrich (1994, figure 11·9) for a channel slope equal to the average channel slope (0·28, Figure 2) of W960 and W1165 and is on the order of the size of the subcatchments themselves. Field evidence, including rooting depths, indicates that little, if any, incision existed in the interface region before the wildfire and flood events.

After delineating the stream network for the composite DEM area, large-scale measurements of topologic stream variables (bifurcation, length, slope and drainage area) were derived from the composite DEM only for those catchments that were largely within the Pikes Peak granite batholith. Spring Creek was an order 6 catchment, so large-scale measurements were derived for 14 order 6 catchments within the batholith for comparison with the small-scale catchment data. This convention allowed us to sample a large part of the batholith as well as having large enough catchments that the derived Horton ratios approached the asymptotic values. In addition to the 14 order 6 catchments, we also compiled separate data for the Spring Creek catchment. Mean values for stream variables (numbers, length, $L$ (m), and drainage area, $A$ ($m^2$)) were computed directly in RiverTools. Extrapolating results from smaller scales to the large scale becomes more uncertain because the variation about the asymptotic values is expected to be greater at smaller scales than at larger scales. Therefore, estimates of this uncertainty were made by calculating the statistics (mean values and coefficients of variation) for the distribution of the Horton ratios ($R_B$, $R_A$ and $R_L$) computed for all catchments (extracted from the composite DEM) within order $j$ catchments (where $j = 2$, 3, 4, 5 or 6).

## Small-scale measurements

Field measurements of stream variables were made in 1999 at 5-m intervals along all the newly incised drainages in the interface region of subcatchments W960 and W1165 as well as along some of the new rills in the hillslope region. Assuming that the post-flood surface adjacent to the rills, gullies and channels was the same as the pre-flood surface,

the volume of material removed from the newly incised drainages was calculated by extending this post-flood surface across the channel, measuring the depth down from this imaginary surface to the bottom of the incised drainage, and multiplying by the average of the top width and bottom width. Identification of the location of the pre-flood surface above the incision was aided in many places by using tree roots left exposed after the floods. These roots and rootlets, typically, were unbroken and in some cases spanned the entire gully or channel. The hydraulic variables included: distance from the mouth, $d$ (m); local channel slope (over a distance equal to 1·82 m), $S$; channel top and bottom width, $w_T$ (m) and $w_B$ (m); channel depth, $h$ (m); channel side slope on both sides (over a distance equal to 0·61 m), $\phi_R$ and $\phi_L$; and the average roughness height $h_b$ (cm), on the channel bed (Moody and Martin, 2001b). Three variables, channel cross-sectional area, $a_x$ (m$^2$), the dimensionless channel width-to-depth ratio, $w_T/h$, and the dimensionless catchment Froude number (ratio of inertial forces to gravitational forces), were derived from field variables. The catchment Froude number is defined (S. D. Peckham, personal communication, 2004) as

$$F = \frac{u}{\sqrt{gH}} \tag{4}$$

where $g$ is the acceleration due to gravity, $H$ (m) is the elevation drop from the beginning of the stream to the end of the stream, and $u$ (m s$^{-1}$) is the mean velocity. The standard Froude number uses the flow depth, $h$, instead of $H$. The mean velocity was estimated assuming the law-of-the-wall for turbulent channel flow, which gives

$$u = \frac{u_*}{\kappa} \ln \frac{h}{ez_0} \tag{5}$$

where $u_* = (ghS)^{1/2}$ is the shear velocity (m s$^{-1}$), $\kappa$ is von Karman's constant equal to 0·408, $e = 2{\cdot}7$, and $z_0$ (m) is the bed roughness parameter, which was set equal to $h_b$ (cm)/10 (JD Smith, personal communication, 2004).

Some topologic variables of the subcatchments (W960 and W1165) were measured from a modified DEM. The modified DEM was produced from topographic maps with a 2-m contour interval created for each subcatchment from a 30-m DEM of the region. The 2-m contours were adjusted to reflect field observations and stereo photographs (1:3000 scale) of the drainage network and ridges. The adjusted contour map was used to create a modified DEM using the ANUDEM algorithm of Hutchinson (1989) as implemented in Arc-Info. This modified DEM, with a grid cell resolution of 1 m$^2$, was then used to estimate upslope-contributing area, $A_c$ (m$^2$), at each measurement location. The upslope-contributing area of the order 1 stream channel head was divided by the channel width to determine the critical area per channel width, $a'_{cr}$ (m) analogous to the critical area defined by Montgomery and Dietrich (1994) for channel initiation but associated with a time scale of an individual rainstorm.

## Results

Measurements derived from the composite DEM do not resolve the small-scale structures measured in the field. Both subcatchments were order 2 catchments in the composite DEM, while based on field measurements W960 and W1165 (despite its smaller size) were order 3 and order 4 catchments respectively. They had drainage areas derived from the composite DEM that were 11 and 24 per cent larger (7·8 and 4·6 ha) than the drainage areas derived from the modified DEM. In contrast, the length of the highest order streams derived from the composite DEM (277 and 162 m) were less than those measured in the field (292 and 223 m).

### Topologic variables

Horton ratios for bifurcation, drainage area, stream length and stream slope were calculated at three scales (subcatchment, Spring Creek and Pikes Peak granite batholith). For the field measurements, the coefficient of determinations ($r^2$, using Equation 2) ranged from 0·96 to 1·00 with the exception of stream length in W1165 ($r^2 = 0{\cdot}86$). The ratios measured at the smaller scales were generally less than those derived from the composite DEM with the exception of $R_A$ for W960 (Table I).

Tokunaga matrices were also calculated for each scale. At the Pikes Peak granite batholith scale, the diagonal elements, $T_{\omega,\omega-1}$, were nearly the same ($1{\cdot}2 \pm 0{\cdot}10$, where the value 0·10 is the coefficient of variation) so that $T_{\omega,\omega-1} \cong T_1$ for all $\omega$ (Table II). These diagonal elements had less variability than those at the smaller Spring Creek scale ($0{\cdot}9 \pm 0{\cdot}50$). This also was true for $T_2$ at the batholith scale ($3{\cdot}4 \pm 0{\cdot}12$), which was less variable than at the Spring Creek scale ($2{\cdot}0 \pm 0{\cdot}63$). The Tokunaga matrix was expanded to include rills (referred to hereafter as order 0 streams)

 

**Table II.** Tokunaga or side tributary matrices for three different scales

| | Order 0 | Order 1 | Order 2 | Order 3 | Order 4 | Order 5 |
|---|---|---|---|---|---|---|
| Pikes Peak granite batholith | | | | | | |
| Order 2 | – | 1·2 | | | | |
| Order 3 | – | 3·7 | 1·1 | | | |
| Order 4 | – | 9·2 | 2·9 | 1·1 | | |
| Order 5 | – | 24·7 | 9·0 | 3·3 | 1·2 | |
| Order 6 | – | 58·4 | 22·8 | 8·4 | 3·8 | 1·4 |
| Spring Creek | | | | | | |
| Order 2 | – | 1·3 | | | | |
| Order 3 | – | 3·6 | 1·1 | | | |
| Order 4 | – | 6·3 | 2·1 | 0·9 | | |
| Order 5 | – | 9·0 | 2·5 | 0·5 | 1·0 | |
| Order 6 | – | 45·0 | 17·0 | 4·0 | 2·0 | 0·0 |
| W960 | | | | | | |
| Order 1 | 6·4 | | | | | |
| Order 2 | 17·6 | 0·5 | | | | |
| Order 3 | 99·0 | 3·0 | 2·0 | | | |
| W1165 | | | | | | |
| Order 1 | 6·7 | | | | | |
| Order 2 | 7·3 | 0·6 | | | | |
| Order 3 | 31·0 | 1·5 | 0·0 | | | |
| Order 4 | 92·4 | 3·0 | 1·0 | 0·0 | | |

Order 0 streams are rills

on the hillslopes at the subcatchment scale (W960 and W1165). At this scale, the number of stream orders is small and the diagonal elements of the modified Tokunaga matrix are not equal (Table II). This indicates that the number of rills, which formed a series of parallel side tributaries into higher order stream channels, was much greater than what would be predicted from the structure of the channel network.

## Hydraulic and dynamic variables

Hydraulic variables were separated into two groups. The Horton ratios for the hydraulic variables of width, depth and cross-sectional area had $r^2$ values between 0·94 and 1·00 with the exception of depth in W1165 ($r^2 = 0{\cdot}69$). The hydraulic variables of bed roughness and width-to-depth ratio, and the dynamic variable (catchment Froude number) were all approximately constant (±1·0) across three to four stream orders and as such had lower $r^2$ values reflecting the lack of correlation with scale.

Numerous hydraulic measurements were made for each stream order, which provided information on the distribution of each topologic and hydraulic variable. Four parameters (mean, coefficient of variation, skewness and kurtosis) were calculated to describe these distributions (Table III). All of the distributions were positively skewed except for the drainage area for the order 2 streams in W1165. The negative kurtosis (flatness of the distribution) was relatively small (<–2·6), while the positive kurtosis (peakedness of the distribution) had a wide range from 0·01 to greater than 20 for cross-sectional area and width-to-depth ratio.

## Critical area for channel initiation

The mean critical area per channel width represents an upper bound on the area necessary to form a channel. The mean values for the 11 order 1 stream channel heads (two of the smallest were not measured) in W960 was 940 m, and for the 18 order 1 stream channel heads (one was not measured) in W1165 was 670 m (Table III). Many order 1 streams began where more than two rills joined. An average of 6·3 rills joined to produce an order 1 stream in W960 and an average of 3·6 rills joined in W1165. In general, these critical areas containing the rills were concave, obovate-shaped surfaces with a group of rills joining at the downslope narrow end to form the order 1 stream channel.

**Table III.** Topologic and hydraulic stream variables of subcatchments W960 and W1165

| | | Number measurements | | Mean | | Coefficient of variation | | Skewness | | Kurtosis | |
|---|---|---|---|---|---|---|---|---|---|---|---|
| **Variable** | **Order** | **W960** | **W1165** | **W960** | **W1165** | **W960** | **W1165** | **W960** | **W1165** | **W960** | **W1165** |
| Number of streams | 0 | – | – | 365 | 378 | – | – | – | – | – | – |
| | 1 | – | – | 13 | 19 | – | – | – | – | – | – |
| | 2 | – | – | 4 | 5 | – | – | – | – | – | – |
| | 3 | – | – | 1 | 2 | – | – | – | – | – | – |
| | 4 | – | – | | 1 | – | – | – | – | – | – |
| Critical area/width (m) | 1 | 11 | 18 | 940 | 670 | 0·75 | 0·90 | 2·2 | 1·7 | 5·4 | 2.3 |
| ln(*a*/*S*) | 1 | 11 | 16[a] | 7·6 | 7·1 | 0·07 | 0·12 | 1 | 0·1 | 1·4 | −1·1 |
| Drainage area (ha) | 1 | 11[a] | 18[a] | 0·20 | 0·06 | 1·20 | 0·85 | 2·8 | 1·6 | 8·4 | 2.4 |
| | 2 | 4 | 4 | 0·95 | 0·27 | 0·69 | 0·56 | – | −1·7 | – | 2.7 |
| | 3 | 1 | 2 | 7·02 | 0·94 | – | 0·35 | – | – | – | – |
| | 4 | – | 1 | – | 3·72 | – | – | – | – | – | – |
| Length (m) | 0 | 36[b] | 38[b] | 27 | 29 | 0·70 | 0·48 | 0·3 | 0·6 | −0·1 | −1·0 |
| | 1 | 13 | 18 | 49 | 55 | 0·69 | 0·56 | 0·9 | 0·9 | 0·1 | −0·4 |
| | 2 | 4 | 5 | 137 | 50 | 0·40 | 0·57 | 1·2 | 0·7 | 1·9 | −2.6 |
| | 3 | 1 | 2 | 292 | 113 | – | 0·16 | – | – | – | – |
| | 4 | – | 1 | – | 223 | – | – | – | – | – | – |
| Slope | 1 | 120 | 172 | 0·41 | 0·40 | 0·24 | 0·29 | 0·50 | 0·20 | 1·4 | −0·4 |
| | 2 | 106 | 42 | 0·34 | 0·35 | 0·35 | 0·43 | 0·78 | 0·7 | 1·0 | 0·8 |
| | 3 | 57 | 47 | 0·22 | 0·30 | 0·18 | 0·53 | 0·16 | 0·9 | −0·8 | −0·1 |
| | 4 | – | 41 | – | 0·22 | – | 0·64 | – | 2·7 | – | 7·4 |
| Width (m) | 0 | 109[b] | – | 0·30 | – | 0·43 | – | 1·3 | – | 1·4 | – |
| | 1 | 120 | 172 | 0·98 | 0·55 | 0·62 | 0·49 | 1·6 | 1·4 | 3·2 | 2.5 |
| | 2 | 106 | 42 | 1·93 | 1·06 | 0·59 | 0·55 | 1·6 | 1·4 | 3·4 | 2·8 |
| | 3 | 57 | 47 | 5·03 | 1·44 | 0·35 | 0·42 | 1·1 | 0·7 | 2·3 | 0·2 |
| | 4 | – | 41 | – | 4·02 | – | 0·30 | – | 0·5 | – | 0 |
| Depth (m) | 1 | 120 | 172 | 0·20 | 0·12 | 0·86 | 0·64 | 1·7 | 1·4 | 2·7 | 1·9 |
| | 2 | 106 | 42 | 0·42 | 0·33 | 0·79 | 0·80 | 1·3 | 1·2 | 1·5 | 0·7 |
| | 3 | 57 | 47 | 0·86 | 0·39 | 0·40 | 0·64 | 1·1 | 1·3 | 1·5 | 2.2 |
| | 4 | – | 41 | – | 0·38 | – | 0·75 | – | 0·7 | – | −0·8 |
| Cross-sectional area ($m^2$) | 1 | 120 | 172 | 0·19 | 0·049 | 1·63 | 0·92 | 4·6 | 3·7 | 25·8 | 23·2 |
| | 2 | 106 | 42 | 0·69 | 0·29 | 1·06 | 1·00 | 1·9 | 0·6 | 3·9 | −0·3 |
| | 3 | 57 | 46 | 4·35 | 0·43 | 0·79 | 0·79 | 3·3 | 1·5 | 13·6 | 2·6 |
| | 4 | – | 41 | – | 1·33 | – | 0·72 | – | 0·8 | – | −0·1 |
| Bed roughness (mm) | 1 | 120 | 163 | 5·5 | 5·2 | 0·61 | 0·69 | 0·9 | 1·1 | −0·3 | 1·0 |
| | 2 | 106 | 36 | 10·4 | 11·8 | 0·64 | 0·62 | 1·1 | 0·6 | 0·5 | −0·3 |
| | 3 | 57 | 27 | 4·8 | 15·9 | 0·50 | 1·02 | 2·4 | 1·3 | 7·1 | 0·6 |
| | 4 | – | 39 | – | 4·7 | – | 1·04 | – | 1·5 | – | 1·7 |
| Width-to-depth ratio | 1 | 120 | 172 | 8·6 | 7·3 | 1·20 | 1·28 | 2·7 | 3·8 | 7·8 | 16·1 |
| | 2 | 106 | 42 | 8·9 | 5·4 | 0·52 | 1·04 | 5·4 | 2·5 | 31·9 | 6·9 |
| | 3 | 57 | 47 | 6·5 | 5·7 | 0·40 | 1·14 | 0·7 | 4·0 | 0·8 | 20·4 |
| | 4 | – | 41 | – | 22·2 | – | 1·09 | – | 2·8 | – | 10·1 |
| Catchment Froude number | 1 | 1 | 1 | 0·46[c] | 0·25[c] | – | – | – | – | – | – |
| | 2 | 1 | 1 | 0·40[c] | 0·46[c] | – | – | – | – | – | – |
| | 3 | 1 | 1 | 0·52[c] | 0·29[c] | – | – | – | – | – | – |
| | 4 | – | 1 | – | 0·36[c] | – | – | – | – | – | – |

–, no data

[a] Areas for 1 or 2 streams were unavailable

[b] Subsample of all the rills

[c] Computed using the mean stream bed roughness, depth, slope and fall, *H*

# Discussion

## Scaling invariant variables

A variable with the absolute value of the Horton ratio equal to 1 indicates a case of scale invariance in which the variable is constant with scale. From a modelling perspective these variables are constants that can be assigned to channels at each scale, a convenient large-scale approximation. The ratio for stream slope ranged from −1·2 to −1·4 across order 1 to order 6 streams (Table I) and the width-to-depth ratios were −1·2 (W960) and 1·4 (W1165) across order 1 to order 4 streams. The Horton ratios for bed roughness, $R_{z_0}$, and catchment Froude number, $R_F$, deviated less from 1 than all the variables. This is not too surprising because the catchment Froude number is weakly dependent on the depth.

To a first approximation $R_{z_0}$ can be modelled as a constant equal to l for all scales. However, on closer inspection of Table III, the bed roughness varies with scale. It was slightly lower for order 1 streams in both subcatchments, increased for mid-order streams (order 2 in W960 and orders 2 and 3 in W1165), and then decreased for the highest order streams (order 3 in W960 and order 4 in W1165). Order 1 streams were gullies closest to the drainage divide, smaller in size (Table III), and incision exposed primarily surficial soil particles ($D_{50} = 2{\cdot}9$ mm on north-facing hillslopes and $D_{50} = 2{\cdot}6$ mm on south-facing hillslopes; Martin and Moody, 2001a). Order 2 and 3 streams were also gullies with relatively narrow channels and width-to-depth ratios typically were less than 10 (Table III). These were incised into the regolith and exposed cobbles and boulder-sized material. In contrast, the order 4 stream (W1165) typically had a width-to-depth ratio greater than 10 with a depositional rather than an erosional bed, which consisted of sand and gravel (0·1–10 mm) particles. This tendency for the bed roughness to decrease downstream is well known (Paola and Seal, 1995), and is controlled by geologic forces rather than fluid forces, which control the width-to-depth ratio and other channel geometry (S. D. Peckham, personal communication, 2004). Thus, it appears that these characteristics of the gully drainage network in the interface region are substantially different from the characteristics of the channel region. However, it does appear that bed roughness, slope, velocity and catchment Froude number remain relatively constant throughout the gully drainage network, and, again to a first approximation, a constant value of each could be used in modelling the drainage network of these lowest-order streams in the interface region.

## Structure of the batholith-scale channels

The three Horton ratios (bifurcation, contributing drainage area and stream length) describe the topological structure of drainage networks. The mean bifurcation ratio for the order 6 catchments in granitic terrain is nearly equal to the value of 4·0 predicted by the random topology model of Shreve (1969). However, the average value of the bifurcation ratio (based on all catchments extracted from the composite DEM within order $j$ catchments) increases asymptotically (Figure 4A) as a function of scale (stream order). It is less than the bifurcation ratios published by Peckham (1995b) for two order 8 catchments (4·6 for a humid and 4·7 for a semi-arid catchment). The values for the order 8 catchments described in Peckham (1995b) are probably closer to the respective asymptotic value for the specific geologic and climatic terrains, while the values for the batholith scale represent an estimate of the asymptotic value with greater uncertainty. Statistical estimates of the ratios for drainage area and stream length decrease rapidly as scale increases from order 2 catchments ($N = 427$) to order 3 catchments ($N = 942$) and then appear to approach an asymptotic value (Figure 4A). The uncertainty (expressed as the coefficient of variation) of each of these ratios decreases rapidly from order 2 to order 6 (Figure 4B). The stabilization of the Horton ratios for drainage area and stream length implies that the uncertainty of choosing a specific critical area is minimized at the order 3 catchment level.

## Structure of the hillslope and interface regions

Before comparing the drainage network in the interface region to its larger-scale counterpart, the channel network described above, it is first necessary to describe the hillslope and interface regions upslope from channel region. The fundamental drainage unit in the hillslope region is the rill, which typically has width-to-depth ratios less than 10 ($7 \pm 1{\cdot}2$, 95 per cent confidence limits; Moody and Martin, 2001b, table 4·8). Rills appeared to be ephemeral on a decadal time scale in the Spring Creek catchment (Pine, 2002) and were observed to have two different spatial patterns. One pattern was nearly parallel rills with a long and narrow drainage area on small-scale segments of hillslopes that approximated a planar surface with constant inclination. Once the critical area or critical discharge for individual rill initiation (Horton, 1945) is exceeded on a planar surface, the flow lines are straight down the hillslope gradient. Water discharge does not accumulate substantially in the downstream direction based on field measurements of other rills that indicate nearly constant cross-sectional area with downstream distance on an approximately planar

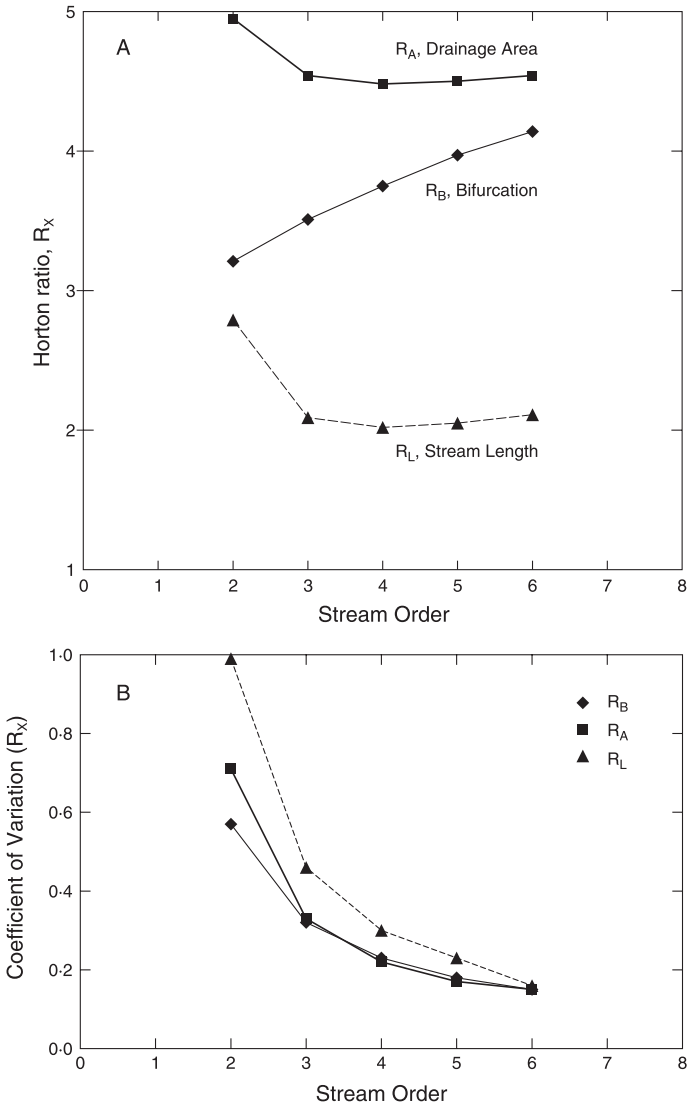


**Figure 4.** (A) Variation of selected Horton ratios as a function of scale (stream order). (B) Coefficient of variation of each Horton ratio shown in (A) as a function of scale. All 4276 order 2 catchments were extracted from the composite DEM and order 1 and order 2 stream properties were used to calculate the expected value and coefficient of variation at the scale of order 2. Similarly, all 942 order 3 catchments were extracted and order 1, 2 and 3 stream properties were used to calculate the expected value and coefficient of variation for the distribution, and likewise for higher order *j* catchments.

surface (Moody and Martin, 2001b, figure 4·7). This is in contrast to channel networks where water discharge can increase abruptly at a channel confluence and the cross-sectional area usually increases downstream. The second pattern was a group of rills that converge together within an obovate-shaped critical area. If the obovate surface of the critical area is divided into triangular segments equal to the number of converging rills, then each rill can be approximated as flow on a small planar surface. At the lower end of the critical area, the water discharge also increases abruptly and forms an order 1 channel.

The analysis of the composite DEM predicts an unburned channel network based on a critical area of 1 ha for order 1 streams. We have hypothesized (see above) that this is the critical area for channel initiation under unburned conditions over long time scales. The consequence of the wildfire was to reduce this critical area by an order of magnitude to 0·06–0·20 ha (Table III) or to a critical area per unit channel width, $a'_{cr}$, of 670–940 m. Thus, as a result of storms that followed the wildfire, the stream channel region (in the pre-fire catchment) expanded into the interface region. The extension of the channel network was in the form of gully incision of the subtle drainages in the interface

 

region. Gullies, with width-to-depth ratios less than 10, became the fundamental drainage unit in the interface region and were the order 1 and 2 drainages in W960 and the order 1, 2 and 3 drainages in W1165.

## Critical area for channel initiation during unsteady flow

The primary cause for gully development in the interface region after wildfire is a change in the critical area for channel initiation. To examine the factors that control the critical area during unsteady flow, we have created a conceptual model. We begin with a brief review of the steady-state model provided by Montgomery and Dietrich (1994) for steady-state Horton overland turbulent flow produced by rainfall excess. This overland flow response is typical of mountainous terrain in convective rainfall regimes. The critical unit discharge $q_{cr}$ ($m^2\ s^{-1}$) is then

$$q_{cr} = (i_r - i)a_{cr} = \frac{\tau_{cr}^{5/3}}{(\rho g)^{5/3} n S^{7/6}} \tag{6}$$

where $\tau_{cr}$ ($N\ m^{-2}$) is the critical shear required to initiate erosion, $i_r$ ($m\ s^{-1}$) is the mean-annual rainfall intensity, $i$ ($m\ s^{-1}$) is the mean-annual infiltration rate, $n$ ($m^{-1/3}s$) is the Manning roughness parameter for the channel, $S$ is the local slope just above the channel head, $\rho$ ($kg\ m^{-3}$) is the density of water, $g$ ($m\ s^{-2}$) is the acceleration due to gravity, and the exponents, 5/3 and 7/6, are a result of assuming a Manning's type roughness resistance equation. Solving for $a_{cr}$ (m) as a function of hydrologic variables gives

$$a_{cr} = \frac{\tau_{cr}^{5/3}}{(i_r - i) n S^{7/6} (\rho g)^{5/3}} \tag{7}$$

Thus, a steeper slope requires less depth of flow and hence less runoff or critical area to provide the critical shear stress to initiate incision. Conversely, a shallow slope is linked to a larger critical area. An increase in rainfall excess ($i_r - i$) by either an increase in rainfall intensity or a decrease in infiltration rate will decrease the critical area, while a decrease in the critical shear stress decreases the critical area.

We must modify this steady-state conceptual framework (developed for long time scale, low-intensity rainfall conditions) to account for the unsteady-flow conditions associated with runoff produced in mountainous terrain by short time scale, high-intensity rainfall. The hillslope roughness controls the time-to-concentration of runoff (Snider, 1972) and thus the peak discharge, $Q_{peak}$. To formulate an unsteady version of Equation 7, we begin with Snider's assumption of a triangular hydrograph to give a semi-empirical equation for unsteady flow

$$Q_{peak} = \frac{2(I_r - I)a'_{cr} w_T}{0{\cdot}5 t_d + 0{\cdot}6 t_c} \tag{8}$$

where $I_r$ (m) is the total precipitation during the storm, $I$ (m) is the total infiltration, $a'_{cr}$ is the critical area associated with an individual storm, $t_d$ (s) is the duration of the storm, and $t_c$ (s) is the time to concentration. The time to concentration can be estimated by using a Manning's form for the resistance equation on the hillslope similar to the form used to derive Equation 6 where the mean velocity down the hillslope, $v$ ($m\ s^{-1}$), is

$$v = n_{hill}^{-1} h_{hill}^{2/3} S^{1/2} \tag{9}$$

where $n_{hill}$ ($m^{-1/3}s$) is Manning's roughness parameter for the hillslope and $h_{hill}$ (m) is the flow depth on the hillslope. By assuming a simple segment of a circle as an approximation for the obovate shape of the critical area, then the hillslope length can be approximated as $L = (a'_{cr} w_T)^{1/2}$, and $t_c$ is

$$t_c = \frac{L}{v} = \frac{n_{hill} (a'_{cr} w_T)^{1/2}}{h_{hill}^{2/3} S^{1/2}} \tag{10}$$

Substitution of Equation 10 into Equation 8, setting $q_{cr} = Q_{peak}/w_T$, and using Equation 6 gives a quadratic equation for the variable $(a'_{cr})^{1/2}$. Retaining only the positive, physical realistic solution and then squaring gives

$$a'_{cr} = \left( \frac{C_5 + \sqrt{C_5^2 + 4C_4}}{2} \right)^2 \tag{11}$$

where $C_4$ and $C_5$ are:

$$C_4 = \frac{0{\cdot}5 t_d \tau_{cr}^{5/3} S^{-7/6}}{2n(I_r - I)(\rho g)^{5/3}} \tag{11a}$$

$$C_5 = \frac{0{\cdot}6 \tau_{cr}^{5/3} S^{-10/6} w_T^{1/2} n_{hill}}{2n(I_r - I)(\rho g)^{5/3} h_{hill}^{2/3}} \tag{11b}$$

Wildfires can alter the vegetative cover, which changes the effective rainfall $I_r$ but also wildfires can change three hydrologic factors that control the critical area for channel initiation. These factors are infiltration, hillslope friction and critical shear stress, and the effects of wildfire on the critical area for channel initiation were determined by varying the values of these three hydrologic factors.

## Sensitivity of the critical area to wildfire

The values of these three hydrologic factors for unburned conditions in forested mountainous terrain are not well known. No values of $h_{hill}$ for natural rainfall conditions are available so that estimates of $h_{hill}$ must be taken from rainfall simulation experiments. However, Abrahams and Parsons (1990) have pointed out that most published values of $h_{hill}$ from rainfall simulations are underestimates because zero depths, at some points across a hillslope, are included in the calculation of $h_{hill}$. Thus, Abrahams and Parsons (1990) indicate that, when the zero depths are not included, the *corrected* value of $h_{hill}$ ranges from 0·00424 to 0·00709 m, and therefore $h_{hill} = 0{\cdot}005$ m was used for these calculations. Hillslope friction is typically 0·50 $m^{-1/3}s$ for woody brush, litter and duff, or shrubland and grassland (Weltz *et al.* 1992; NRCS, 1986). Critical shear stresses measured for agricultural soils range from about 0·8 to 6·5 N $m^{-2}$ (Elliot *et al.*, 1989), and Dietrich *et al.* (1992) reported values that range from 20 to 100 N $m^{-2}$ for saturated overland flow on grasslands. Dietrich *et al.* (1992) assumed laminar flow and a critical area proportional to $\tau_c^3$. It is unclear whether or not these higher critical shear stresses also include form drag from grass stems and grass clumps, which can be appreciable and should be subtracted to obtain the critical shear stress available for sediment erosion. In general, forested mountainous areas do not have vegetative mats characteristic of grasslands, so that 4 N $m^{-2}$ was selected to represent the 'unburned' conditions. Values of $w_T$, $t_d$, $\rho$ and $g$ were fixed at 1 m, 3600 s, 1000 kg $m^{-3}$, and 9·8 m $s^{-2}$ respectively. Thus, the estimated relation between critical area and slope for unburned conditions ($I_r - I = 0{\cdot}1$ mm $n_{hill} = 0{\cdot}50$ $m^{-1/3}s$ and $\tau_{cr} = 4$ N $m^{-2}$) is shown in Figure 5 as curve A. The rainfall excess (essentially the infiltration factor) is also uncertain and was selected to approximate the trend of the data reported by Montgomery and Dietrich (1994) for unburned grassland and forested catchments.

*Infiltration.* After a wildfire, both chemical and physical changes in the soil (DeBano, 2000) and surface sealing by ash (Mallik *et al.*, 1984) and soil particles (Neary *et al.*, 1999) are attributed to changes in water repellency. The change is usually a decrease in the infiltration rate, which would increase the term $(I_r - I)$ in Equation 11. The effect of reducing infiltration by wildfire is estimated by curve B (Figure 5) where the term $I_r - I$ has been increased 200 times but the other factors remain unchanged. This change could represent decreased infiltration or increased effective rainfall because the vegetation cover has been removed by burning. It could also be the effect of reduced infiltration coupled with the possibility of an unusual rainfall on the order of a 100-year recurrence interval. This lowers the curve relative to the unburned condition by about three orders of magnitude. Wildfire effects on infiltration have been measured in mountainous terrain and indicate a decrease by about a factor of four to seven (Martin and Moody, 2001b). Median maximum 30-minute intensity in the Spring Creek catchment for 4 years after the wildfire in 1996 was about 1·1 mm $h^{-1}$, while the storm that caused the gully erosion was about 100 times greater (Moody and Martin, 2001b). Therefore, the character of the rainfall may be more important than the change in infiltration rate.

*Hillslope friction.* Fires decrease the hillslope friction by removing obstructions, which reduces the friction to values typical of bare soil ($n_{hill} = 0{\cdot}01$ $m^{-1/3}s$; Weltz *et al.*, 1992; NRCS, 1986). A consequence of removing these obstructions is that the time for runoff to reach the channel decreases. The effect of reducing the hillslope friction by approximately a factor of 50 ($n_{hill} = 0{\cdot}50 \rightarrow 0{\cdot}01$ $m^{-1/3}s$) is shown by curve C (Figure 5) and has much less effect than changing the excess rainfall.

*Critical shear stress.* The critical shear stress, $\tau_{cr}$ for cohesive forest soils depends on the temperatures to which the soil is exposed during a wildfire. For 'unburned' soils the critical shear stress is about 2 N $m^{-2}$, similar to the unburned critical shear stresses mentioned above. The critical shear stress reaches a maximum (>3·2 N $m^{-2}$) between 200 and 250 °C for 'burned soils' and decreases rapidly to about 0·5 N $m^{-2}$ for soils exposed to temperatures greater than 250 °C (Moody *et al.*, 2005). Curve D (Figure 5) illustrates the effect of reducing the critical shear stress from 4 to 0·5 N $m^{-2}$. This reduces the critical area by about one order of magnitude.

 

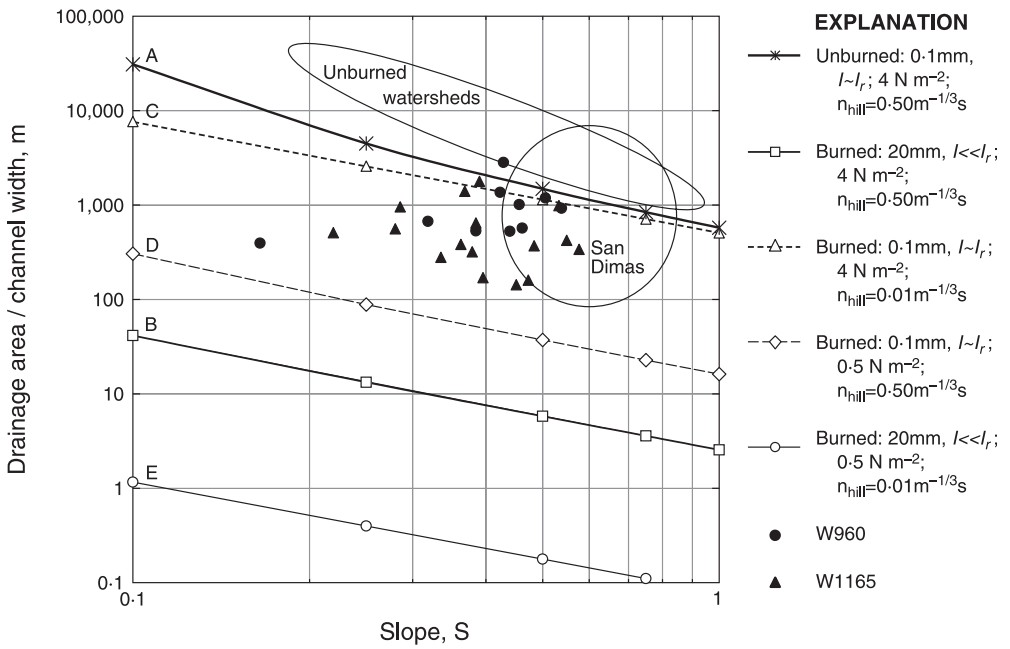


**Figure 5.** Drainage area per unit channel width upstream from an order 1 stream is shown as a function of slope at the beginning of each order 1 stream. Curve A represents the unburned condition ($\tau_{cr} = 4$ N m$^{-2}$, $I_r - I = 0{\cdot}1$ mm and $n_{hill} = 0{\cdot}50$ m$^{-1/3}$s). Curve B is a burned condition with only a change in the total infiltration rate, $I$, such that it is much less than the total rate, $I_r$ ($\tau_{cr} = 4$ N m$^{-2}$, $I_r - I = 20$ mm and $n_{hill} = 0{\cdot}50$ m$^{-1/3}$s). Curve C is a burned condition with only a decrease in the hillslope friction parameter ($\tau_{cr} = 4$ N m$^{-2}$, $I_r - I = 0{\cdot}1$ mm and $n_{hill} = 0{\cdot}01$ m$^{-1/3}$s). Curve D is a burned condition with only a decrease in the critical shear stress ($\tau_{cr} = 0{\cdot}5$ N m$^{-2}$, $I_r - I = 0{\cdot}1$ mm and $n_{hill} = 0{\cdot}50$ m$^{-1/3}$s). Curve E is a burned condition with changes in all three variables: infiltration, hillslope friction and critical shear stress ($I_r - I = 20$ mm, $n_{hill} = 0{\cdot}01$ m$^{-1/3}$s and $\tau_{cr} = 0{\cdot}5$ N m$^{-2}$).

*Combined factors*. Wildfires produce a variety of combinations of changes in infiltration, hillslope friction and critical shear stress. A worst-case scenario is shown by curve E (Figure 5). Change of the critical shear stress by fire appears to have the largest effect on the critical area. Changes in the infiltration rate by fire appear to have a large effect only if $I_r \sim I$, but then $I_r - I \sim 0$ and the runoff is approximately zero. If $I_r \gg I$, then the change in critical area is large; however, this is not simply a consequence of wildfire but the consequence of a rainstorm with a large return interval, which also would affect unburned catchments.

## Critical area for burned catchments

The critical area per channel width for channel initiation in the burned catchments appears to be independent of slope. These areas are definitely less than the areas with corresponding slopes in the unburned catchments (Figure 5) and probably represent some combination of changes in infiltration, hillslope friction and critical shear stress, but also include the effect of changes in vegetative cover. The effect of different vegetation cover on the critical area was observed by Vandekerckhove *et al*. (2000) in cultivated fields and rangeland in Mediterranean Europe. The San Dimas data (Montgomery and Dietrich, 1994) for tectonically active, granitic terrain frequently burned by wildfires in southern California indicates that, in general, the critical area also is less than the value for the grasslands catchments and similar to those for this study of burned mountainous catchments.

Recall that the critical area per channel width, $a'_{cr}$, in the burned area is defined by unsteady flow associated with convective storm-type rainfall conditions (short time scale, high-intensity rainfall) while the critical area per channel width, $a_{cr}$, in the unburned areas is defined by mean annual rainfall conditions (long time scale, low-intensity rainfall conditions). An important distinction specific to some of the unburned catchments reported by Montgomery and Dietrich (1994) is that the overland flow process is different from that for burned catchments. The critical areas associated with saturated overland laminar flow, characteristic of many unburned catchments, are larger than those for rainfall excess overland turbulent flow characteristic of burned areas. An important question is whether the entire

 

critical area defined by unsteady rainfall excess overland flow and the entire critical area defined by steady-state saturated overland flow contribute water to create an incised channel. If they do not, then these critical areas may fit either the partial contributing area model proposed by Betson (1964) for infiltration excess overland flow, or a similar model proposed by Hewlett and Hibbert (1967) for saturated excess overland flow, and represent areas larger than is necessary to initiate a channel. Based on the relatively small size of $a'_{cr}$ and our observations in burned catchments, we feel that the entire critical area, $a'_{cr}$ does contribute to channel initiation.

The critical area, however, is not a fully robust way of distinguishing channels from non-channel areas. If the small critical area observed in this study of burned catchments were actually applied to an appropriately scaled DEM, then there would be channels throughout the entire catchment (see for an example Sun *et al*., 1994, figure 6), which was definitely not observed in the field. The fact that all critical areas were within a concave, obovate area suggests that hillslope curvature may be an important additional property to consider. The topographic parameter $\ln(a/S)$ includes both area and slope and identifies regions of curvature often referred to as *hollows* (Dietrich and Dunne, 1978). The mean value of the $\ln(a'_{cr}/S)$ parameter for order 1 channel heads in W960 was $7{\cdot}6 \pm 0{\cdot}07$ ($\pm$ coefficient of variation) and in W1165 it was $7{\cdot}1 \pm 0{\cdot}12$. This parameter is nearly constant and has much less variation than either the critical area or slope (Table III). This suggests that $\ln(a'_{cr}/S)$ should be considered when modelling the distribution of order 1 channels.

## Predicting small-scale channel structure

The significance of scale invariance for modelling is that the small-scale drainage structure (not resolved at the composite DEM scale) can be predicted by either the Tokunaga matrix or the Horton ratios derived from the large-scale drainage structure, provided the structures of the drainage networks are the same. To test this, the number of streams, drainage areas and stream lengths were predicted for the small-scale drainage network in the interface and hillslope regions of the burned catchments by using results from the composite DEM. For stream numbers, both the Horton bifurcation ratio and the Tokunaga matrix were used, and for drainage areas and stream lengths the Horton ratios were used. We expected that the Tokunaga matrix would be more accurate because it includes quasi-two-dimensional properties and does not change systematically with scale (S. D. Peckham, personal communication). The predicted values of stream variables for the two subcatchments are reasonably similar when you consider that the magnitudes are small and thus the percentage differences are relatively large (Table IV). The predicted stream lengths for W960 ranged from 12 per cent longer to 11 per cent shorter than the measured stream lengths, whereas the predicted stream lengths for W1165 were all shorter than the measured stream lengths, especially for the lower stream orders. The predicted number of streams using the Tokunaga matrix method (assuming constancy of diagonals) is closer to the measured number of streams than the predicted number of streams using the Horton bifurcation ratio. Results from both methods indicate that subcatchment W960 fits the self-similar hypothesis better than W1165, which appears to be anomalous in that the predicted number of order 1, 2 and 3 streams is much lower than the measured number of streams.

The question is whether the documented changes in critical area per unit contour affect the structure of the drainage network that develops after wildfire when compared to the large-scale drainage network. Sun *et al*. (1994) have shown that the number of order 1 and 2 streams in theoretical optimal channel networks (for mean annual rainfall conditions) is dependent on the inclusion of the processes implied by using a critical area for the hillslope region. A *hillslope effect ratio* can be defined to be equal to the number of streams in the catchment without hillslope processes (critical area = 0) divided by the number of streams for the catchment with hillslope processes. For a theoretical catchment (with a hillslope inclination of 30 °), the theoretical ratios were 1·8, 1·1 and 1·0 for order 1, 2 and 3 streams (Sun *et al*., 1994, figure 6). A similar ratio can be calculated from our field data to verify this prediction for storm rainfall conditions. It is the number of streams predicted by using the Tokunaga matrix divided by the measured number of streams. The hillslope effect ratios for W960 are then 1·1, 0·8 and 1·0, which are similar to the theoretical hillslope effect ratios. For W1165 the hillslope effect ratios (3·3, 2·8 and 1·5) are larger. These results suggest that the hillslope region (in these subcatchments and perhaps in catchments in general) may have a secondary effect in determining the distribution of order 1 channels and may reduce in some cases the number of order 1 and even order 2 streams needed to efficiently drain water from the catchment compared to the number predicted by primary topological properties of the larger channel network.

The possible reduction in the number of order 1 and order 2 streams is a secondary effect and it could be interpreted to indicate that the mean self-similar structure of the channel region does not extend ubiquitously into the interface regions. However, it should be noted that the bifurcation structure of lower order basins (see Figure 4) is variable, and the bifurcation ratios for the subcatchments are within the standard deviation of bifurcation ratios of second-order catchments. Still, it appears that the structure of the hillslope drainage network composed of multiple rills may serve

 

**Table IV.** Comparison of the predicted channel variables at the small subcatchment scale with the measured variables

| | W960 | | | W1165 | | |
|---|---|---|---|---|---|---|
| **Order** | **Predicted** | **Measured** | **Difference (%)** | **Predicted** | **Measured** | **Difference (%)** |
| Tokunaga matrix method, $T_1 = 1{\cdot}2$, $T_2 = 3{\cdot}4$, $T_3 = 8{\cdot}9$ | | | | | | |
| Number of streams | | | | | | |
| 0 | 63 | 365 | –83 | 301 | 378 | –20 |
| 1 | 14 | 13 | 8 | 63 | 19 | 232 |
| 2 | 3 | 4 | –25 | 14 | 5 | 180 |
| 3 | 1 | 1 | – | 3 | 2 | 50 |
| 4 | | | | 1 | 1 | – |
| Horton ratio method | | | | | | |
| $R_B = 4{\cdot}3$ | | | | | | |
| Number of streams | | | | | | |
| 0 | 80 | 365 | –78 | 342 | 378 | –10 |
| 1 | 18 | 13 | 38 | 80 | 19 | 321 |
| 2 | 4 | 4 | 0 | 18 | 5 | 260 |
| 3 | 1 | 1 | – | 4 | 2 | 100 |
| 4 | | | | 1 | 1 | – |
| $R_A = 4{\cdot}8$ | | | | | | |
| Drainage area (ha) | | | | | | |
| 0 | 0·06 | – | – | 0·01 | – | – |
| 1 | 0·30 | 0·20 | 50 | 0·03 | 0·06 | –50 |
| 2 | 1·46 | 0·95 | 54 | 0·16 | 0·27 | –41 |
| 3 | 7·02 | 7·02 | – | 0·77 | 0·94 | –18 |
| 4 | | | | 3·71 | 3·71 | – |
| $R_L = 2{\cdot}3$ | | | | | | |
| Stream length (m) | | | | | | |
| 0 | 24 | 27 | –11 | 8 | 29 | –72 |
| 1 | 55 | 49 | 12 | 18 | 55 | –67 |
| 2 | 127 | 137 | –7 | 42 | 50 | –16 |
| 3 | 292 | 292 | – | 97 | 113 | –14 |
| 4 | | | | 223 | 223 | – |

Tokunaga matrix and Horton ratios were derived from the larger batholith scale (30-m DEM)

to replace the need for as many order 1 streams to satisfy the space-filling requirement of theoretical stream channel networks. The hillslope drainage structure is perhaps less efficient than the channel network but it may decrease the number of order 1 and order 2 channels. Its inclusion in the field measurements may explain why the fractal dimensions for the subcatchments are less than 2, while the fractal dimension computed at the batholith scale is closer to 2. While the secondary hillslope effect has yet to be incorporated into the Tokunaga matrix, using the Tokunaga matrix (at the present time) provides the best method for predicting the number of small-scale, order 1 and order 2 channels in the interface region. It must be remembered that these order 1 and order 2 channels in the interface region are not resolved by the large-scale 30-m DEM and thus are not equivalent to order 1 and order 2 channels identified by a large-scale analysis.

## Differences between subcatchments

The differences in the predicted channel characteristics of W960 and W1165 can be considered as a tertiary effect representative of the variance of the structure for small catchments in natural channel systems (Figure 4B). However, the differences also may be related to the differences in north- and south-facing hillslopes that have been documented elsewhere. Moody and Martin (2001b) have highlighted many of these differences including different sediment yields from hillslope sediment traps on north-facing from those on south-facing slopes. Soil classifications indicate that soils on north-facing slopes remain frozen and are likely wetter later in the year. These moisture

differences then affect relative infiltration and the types of vegetation on north- and south-facing aspects both before and after a fire. These differences in the annual hydrologic cycle may affect the long-term erosional development of the terrain.

The possible drainage differences between north- and south-facing aspects that were observed in the field measurements of the two catchments were investigated using other order 2 catchments within the composite DEM. We examined the network structure of 17 south-facing order 2 catchments and 16 north-facing order 2 catchments within the order 6 Spring Creek catchment. The results indicated differences in most stream variables but they were not statistically significant except for the shape of the catchment or basin shape. To examine basin shapes, we used a shape factor (Peckham, 1995b) defined as:

$$Sf = \frac{\sqrt{A}}{D} \tag{12}$$

where $A$ ($m^2$) is the drainage area and $D$ (m) is the diameter or the greatest length between any two points on the catchment boundary. North-facing catchments had a significantly ($p = 0{\cdot}077$) lower mean shape factor (0·53) than south-facing catchments (0·57). This implies that north-facing catchments are slightly more elongated than south-facing catchments. North-facing catchments also had a higher average bifurcation number (4·3) than south-facing catchments (3·4) although both distributions are variable ($p = 0{\cdot}22$). Overall, this tertiary effect indicates that the north-facing catchments are elongated and drained by more side tributaries. Although this local examination of north and south differences is not exhaustive, it implies that there may be differences in the way that north- and south-facing catchments develop, which is evident at both the field and composite DEM scales.

## Conclusions

Future process models of runoff from burned catchments need to incorporate the different drainage characteristics of the hillslope, interface and channel regions, and the unsteady nature of runoff created by spatially and temporally variable rainfall. In general, an initial, primary simplification for modelling runoff after fires is that the self-similar scaling laws measured for large-scale channel networks (1–1000 $km^2$) in unburned catchments can be used to predict the small-scale channel network region (0·001–1 $km^2$) not resolved at the large scale. An additional primary simplification is that the topologic (stream slope), hydraulic (width-to-depth ratio and bed roughness) and dynamic (catchment Froude number) variablles can be modelled as scale invariant across three to six stream orders.

In contrast to the simplifications mentioned above, the smaller-scale drainage networks of the hillslope and interface region cannot be predicted from the topologic properties derived from large-scale channel networks and thus, these networks need to be modelled differently. Runoff generated on burned hillslopes is collected by rills, the fundamental drainage unit, and can be modelled with a width-to-depth ratio less than 10. Rills were observed to have two spatial patterns that either drain planar surfaces in a nearly parallel pattern or drain a critical area funnelling water into an order 1 stream as a group of three to six converging rills. The consequence of this hillslope drainage structure is to cause a decrease (a secondary correction) in the number of order 1 and 2 streams in the interface region from what would be predicted from the primary topologic properties of the large-scale channel network.

The fundamental drainage unit in the interface region for burned conditions is the gully. We found that gullies created in granitic terrain can be modelled with a width-to-depth ratio less than 10, a maximum bed roughness relative to the hillslope and channel regions, and a critical area per unit channel width on the order of 670–940 m. This critical area for channel initiation is less than that for unburned conditions and the decrease was primarily a result of a change in the runoff process and in the critical shear stress. Using this critical area per unit channel width to model the distribution and number of gullies would produce much higher drainage densities than we observed in the field. Thus, we suggest that the topographic parameter $\ln(a'_{cr}/S)$ may be a better parameter to use to model the distribution and number of gullies or order 1 channels in the interface region.

The prediction of the distribution of order 1 channels is a critical need for correctly modelling the collection and concentration of water into the expanded and existing channel network. The critical area, $a'_{cr}$, appears to predict an unrealistically large number of order 1 channels while the Tokunaga matrix provides, at present, a practical method of estimating a reasonable upper bound. Probably this number will be reduced when the actual linkage between hillslope drainage processes and order 1 channels is better understood. Understanding this linkage is then a critical step to ensure that unsteady flood flow is correctly modelled and that accurate models can then be constructed of the consequential erosion, sediment transport, and deposition in burned catchments.

 

## Acknowledgments

Part of the work was supported by a Mendenhall Post-Doctoral Fellowship provided to David Kinner. Field measurements at this detail can never be done alone. Tanya Ariowitsch, Lisa Pine and Deborah Martin contributed patience, time and suggestions that made the data collection successful. Lengthy discussions with Deborah Martin, Scott Peckham and Jim Smith clarified many concepts. The use of trade, product or firm names in this paper is for descriptive purposes only and does not constitute endorsement by the US Geological Survey.

## References

Abrahams AD, Parsons AJ. 1990. Determinging the mean depth of overland flow in field studies of flow hydraulics. *Water Resources Research* **26**(3): 501–503.

Andrle R, Abrahams AD. 1989. Fractal techniques and the surface roughness of talus slopes. *Earth Surface Processes and Landforms* **14**(3): 197–209.

Betson RP. 1964. What is watershed runoff? *Journal of Geophysical Research* **69**(8): 1541–1552.

Beven KJ, Kirkby M. 1979. A physically-based variable contributing area model of basin hydrology. *Hydrological Sciences Bulletin* **24**: 43–69.

Blair RW Jr. 1976. Weathering and geomorphology of the Pikes Peak Granite in the southern Rampart Range, Colorado. In *Professional Contributions of Colorado School of Mines*, Epis RC, Weimer RJ (eds). Studies in Colorado Field Geology **8**: 68–72.

Blosch G. 1999. Scaling issues in snow hydrology. *Hydrological Processes* **13**: 2149–2175.

DeBano LF. 2000. The role of fire and soil heating on water repellency in wildland environments: a review. *Journal of Hydrology* **231–232**: 195–206.

Dietrich WE, Dunne T. 1978. Sediment budget for a small catchment in mountainous terrain. *Zeitschrift für Geomorphologic N.F. Suppl. Bd.* **29**: 191–206.

Dietrich WE, Wilson CJ, Montgomery DR, Mckean J, Bauer R. 1992. Erosion thresholds and land surface morphology. *Geology* **20**: 675–679.

Dodds PS, Rothman DH. 2000. Scaling, universality, and geomorphology. *Annual Review of Earth and Planetary Science* **28**: 571–610.

Elliot WJ, Liebenow AM, Laflen JM, Kohl KD. 1989. *A compendium of soil erodibility data from WEPP cropland soil field erodibility experiments 1987 & 88*. US Department of Agriculture, NSERL Report No. 3. Ohio State University and USDA Agricultural Research Service.

Green G. 1992. *The digital geologic map of Colorado in ARC/INFO Format*. US Geological Survey Open-File Report, 92-0507.

Hack JT. 1957. *Studies of longitudinal stream profiles in Virginia and Maryland*. US Geological Survey Professional Paper 294-B.

Hewlett JD, Hibbert AR. 1967. Factors affecting the response of small watersheds to precipitation in humid areas. In *Forest Hydrology*, Sopper WE, Lull HW (eds). Pergamon Press: New York; 275–290.

Horton RE. 1945. Erosional development of streams and their drainage basins; hydrophysical approach to quantitative morphology. *Bulletin of the Geological Society of America* **56**: 275–370.

Howard AD. 1990. Theoretical model of optimal drainage networks. *Water Resources Research* **26**(9): 2107–2117.

Hutchinson MF. 1989. A new method for gridding elevation and stream line data with automatic removal of pits. *Journal of Hydrology* **106**: 211–232.

Interagency Advisory Committee on Water Data. 1981. *Guidelines for determining flood flow frequency*. US Geological Survey Bulletin 17B.

Jennings ME, Thomas WO Jr., Riggs HC. 1994. *Nationwide summary of US Geological Survey regional regression equations for estimating magnitude and frequency of floods for ungaged sites, 1993*. US Geological Survey Water-Resources Investigations Report 94-4002.

Jenson SK, Domingue JO. 1988. Extracting topographic structure from digital elevation data for geographic-information system analysis. *Photogrammetric Engineering and Remote Sensing* **54**(11): 1593–1600.

Kirchner JW. 1993. Statistical inevitability of Horton's laws and the apparent randomness of stream channel networks. *Geology* **21**: 591–594.

Knighton, D. 1998. Fluvial Forms and Processes. A New Perspective. Oxford University Press. Inc., New York 400.

Leopold LB, Langbein WB. 1962. *The concept of entropy in landscape evolution*. US Geological Survey Professional Paper 500-A.

Mallik AU, Gimingham CH, Rahman AA. 1984. Ecological effects of heather burning, I. Water infiltration, moisture retention and porosity of surface soil. *Journal of Ecology* **72**: 767–776.

Mandelbrot BB. 1967. How long is the coast of Britain: Statistical self-similarity and fractional dimension. *Science, New Series* **156**(3775): 636–638.

Martin DA, Moody JA. 2001a. The flux and particle size distribution of sediment collected in hillslope traps after a Colorado wildfire. In *Proceedings of the Seventh Federal Interagency Sedimentation Conference*, 25 to 29 March 2001: III-40 to III-47.

Martin DA, Moody JA. 2001b. Comparison of soil infiltration rates in burned and unburned mountainous watersheds. *Hydrological Processes* **15**: 2893–2903.

Montgomery DR, Dietrich WE. 1994. Landscape dissection and drainage area-slope thresholds. In *Process Models and Theoretical Geomorphology*, Kirkby MJ (ed.). John Wiley & Sons: Chichester; 221–246.

 

Moody JA, Martin DA. 2001a. Initial hydrologic and geomorphic response following a wildfire in the Colorado Front Range. *Earth Surface Processes and Landforms* **26**: 1049–1070.

Moody JA, Martin DA. 2001b. *Hydrologic and sedimentologic response of two burned watersheds in Colorado*. US Geological Survey Water-Resources Investigation Report 01-4122.

Moody JA, Troutman BM. 2002. Characterization of the spatial variability of channel morphology. *Earth Surface Processes and Landforms* **27**: 1251–1266.

Moody JA, Smith JD, Ragan BW. 2005. Critical shear stress for erosion of cohesive soils subjected to temperatures typical of wildfires, submitted to *Journal Geophysical Research, Earth Process*, **110**, F01004. DOI:10.1029/2004JF000141, 1–13.

Moore R. 1992. *Soil Survey of Pike National Forest, Eastern Part, Colorado, Parts of Douglas, El Paso, Jefferson, and Teller Counties*. US Department of Agriculture, Forest Service and Soil Conservation Service.

Neary DG, Klopatek CC, DeBano LF, Ffolliott PF. 1999. Fire effects on below ground sustainability: a review and synthesis. *Forest Ecology and Management* **122**: 51–71.

NRCS. 1986. *Urban hydrology for small watersheds*. US Department of Agriculture, Technical Release 55 (2nd edn).

O'Callahan J, Mark D. 1984. The extraction of drainage networks from digital elevation data. *Vision and Graph. and Image Processes* **28**(3): 323–344.

Paola C, Seal R. 1995. Grain size patchiness as a cause of selective deposition and downstream fining. *Water Resources Research* **31**(5): 1395–1407.

Peckham SD. 1995a. *Self-similarity in the three-dimensional geometry and dynamics of large river basins*. PhD Thesis, University of Colorado.

Peckham SD. 1995b. New results for self-similar trees with applications to river networks. *Water Resources Research* **31**(4): 1023–1029.

Peckham SD. 1998. Efficient extraction of river networks and hydrologic measurements from digital elevation data. In *Stochastic Methods in Hydrology: Rain, Landforms and Floods*, Barndorff-Nielsen *et al.* (eds). World Scientific: Singapore; 173–203.

Peckham SD, Gupta VK. 1999. A reformulation of Horton's laws for large river networks in terms of statistical self-similarity. *Water Resources Research* **35**(9): 2763–2777.

Pine EJ. 2002. *Short-term rill evolution following the Buffalo Creek Fire, Buffalo Creek, Colorado*. Masters Thesis, Department of Natural Science, Mathematics, and Engineering, University of Denver.

Rodriguez-Iturbe I., Rinaldo A. 1997. *Fractal River Basins Chance and Self-Organization*. Cambridge University Press: New York.

Rivix LLC. 2001. *RiverTools User's Guide release 2001*. Research Systems, Inc.: Boulder, Colorado.

Shreve RL. 1966. Statistical law of stream numbers. *Journal of Geology* **74**: 17–37.

Shreve RL. 1969. Stream lengths and basin areas in topologically random channel networks. *Journal of Geology* **77**: 397–414.

Snider D. 1972. *National Engineering Handbook, Section 4 Hydrology*. US Department of Agriculture, National Resource Conservation Service.

Strahler AN. 1957. Quantitative analysis of watershed geomorphology. *Eos Transactions AGU* **38**: 913–920.

Sun T, Meakin P, Jøssang T. 1994. A minimum energy dissipation model for drainage basins that explicitly differentiates between channel networks and hillslopes. *Physica A* **210**: 24–47.

Tokunaga E. 1978. *Consideration on the composition of drainage networks and their evolution*. Geography Report 13. Tokyo Metropolitan University.

Troutman BM, Karlinger MR. 1994. Statistical inevitability of Horton's laws and the apparent randomness of stream channel networks: Comment and Reply. *Geology* **22**(6): 573–575.

Tucker GE, Bras RL. 1998. Hillslope processes, drainage density, and landscape morphology. *Water Resources Research* **34**(10): 2751–2764.

Vail JE. 2000. *Analysis of the magnitude and frequency of floods in Colorado*. US Geological Survey Water-Resources Investigations Report 99-4190.

Vandekerckhove L, Poesen J, Oostwoudwijdenes D, Nachtergaele J, Kosmas C, Roxo MJ, Figueiredo TDE. 2000. Thresholds for gully initiation and sedimentation in Mediterranean Europe. *Earth Surface Processes and Landforms* **25**: 1201–1220.

Welter SP. 1995. *Topographic influences on erosion and soil development in hollows of the Rampart Range, Colorado*. PhD Dissertation, Department of Geography, University of Colorado, Boulder.

Weltz MA, Arslan AB, Land LJ. 1992. Hydraulic roughness coefficients for native rangelands. *Journal of Irrigation and Drainage Engineering* **118**(5): 776–789.

 